CHEMICAL ENGINEERING TRANSACTIONS
VOL. 94, 2022
A publication of AIDIC
The Italian Association of Chemical Engineering
Online at www.cetjournal.it
Guest Editors: Petar S. Varbanov, Yee Van Fan, Jiří J. Klemeš, Sandro Nižetić

ISBN 978-88-95608-93-8; **ISSN** 2283-9216
DOI: 10.3303/CET2294050

Energy Density Optimization in a Primary Alkaline Battery using Multiphysics Modeling

Michael T. Castro, Julie Anne D. Del Rosario, Joey D. Ocon*

Laboratory of Electrochemical Engineering (LEE), Department of Chemical Engineering, University of the Philippines Diliman, Quezon City 1101, Philippines
jdocon@up.edu.ph

Primary alkaline batteries have been widely used in portable electronics due to their low cost and safety. The consumption and disposal of these batteries has prompted notable research on their recycling. Another approach to reducing alkaline battery disposal is to extend their lifetime by increasing their energy density. In this work, the energy density of an AA primary alkaline battery was maximized by determining the optimum amount of electrode materials through multiphysics modeling. An electrochemical model of the alkaline battery is developed in COMSOL Multiphysics® and validated with discharge curves (i.e., voltage vs. time) obtained under constant resistance loads. The electrode thicknesses are then optimized to maximize the energy density of the battery while maintaining its exterior dimensions. The sensitivity of the energy density with respect to the electrode porosities and interfacial areas is then analyzed. The electrochemical model was able to replicate the discharge curves obtained under a 250 mA constant current discharge. The energy density is maximized by decreasing the thickness of the zinc anode. However, this results in anode dissolution near the current collectors and could compromise the electrical continuity in the battery. Increasing the anode thickness prevents dissolution at the current collectors but increases unused mass in the battery. The results of this study can be used to develop longer-lasting alkaline batteries. Furthermore, the model can be improved by considering thermal effects or modified to aid the development of rechargeable alkaline batteries.

1. Introduction

The Zn-MnO_2 primary alkaline battery has been widely used in portable low-power electronics, such as toys, radios, and flashlights. It has dominated the market for single-use batteries, and its global market is expected to grow by USD 494 million from 2020 to 2024 (Business Wire, 2020). Unfortunately, 90% of used primary alkaline batteries end up in landfills due to their disposable nature (Edison et al., 2019). This has prompted research on the recovery of valuable metals from spent primary alkaline batteries (Rarotra et al., 2020) and the redesign of Zn-MnO_2 into a rechargeable chemistry for grid-scale storage (Seo et al., 2018).

An alternative paradigm for increasing the utility of a primary alkaline battery is to maximize its energy density, which can be achieved by optimizing the allocation of materials in the battery. This type of research has been successfully performed for other battery chemistries via multiphysics modeling, which simulates a battery based on fundamental laws in physics and chemistry. The model can then be optimized according to an objective function, such as energy density. Hosseinzadeh et al. (2017) determined the thicknesses and porosities of electrodes in a lithium-ion battery to maximize its energy and power density.

Moreover, multiphysics models can determine the distribution of quantities such as the concentration, temperature, potential, material usage, and porosity in a battery. This lends insights on how the battery design can be improved. For instance, Samba et al. (2014) used the electrode usage and temperature profiles in a Li-ion battery to ascertain the best orientation and width of the current collector tabs in a lithium-ion battery. Alagheband et al. (2017) designed current collector grids for lead-acid batteries to improve the uniformity of the electrode potential and reaction current density.

Multiphysics models have been developed for primary alkaline batteries. Notable contributions include the work of Sunu and Bennion (1980), in which the transport of zinc ions in zinc anodes were described, and the study of Podlaha and Cheh (1994), wherein a multiphysics model of the Zn-MnO_2 primary alkaline battery was

Paper Received: 01 April 2022; Revised: 13 April 2022; Accepted: 18 April 2022
Please cite this article as: Castro M.T., Del Rosario J.A.D., Ocon J.D., 2022, Energy Density Optimization in a Primary Alkaline Battery using Multiphysics Modeling, Chemical Engineering Transactions, 94, 301-306 DOI:10.3303/CET2294050

presented. There has also been interest from the industry to design batteries via multiphysics modeling, with Chadderdon and Wendling (2019) from Energizer Holdings Inc. presenting their primary alkaline battery model to the 2019 COMSOL Conference. Despite the numerous efforts on modeling primary alkaline batteries, however, their optimization has yet to be performed.

In this work, the energy density of an AA primary alkaline battery was maximized via multiphysics modeling. A multiphysics model of the battery was formulated in COMSOL Multiphysics® and validated with experimental data. The operating mechanism (i.e., reactions and ion transport) of the battery over time was inferred by analyzing the porosity and concentration profiles. Afterwards, batteries with varying anode and cathode thicknesses were simulated, and the corresponding energy densities were calculated. The porosity profiles in these alternative scenarios were also compared with those in the base scenario to reveal any changes in the operating mechanisms. This study demonstrates the use of multiphysics modeling for maximizing the performance of a primary alkaline battery, since design optimization was not performed in previous studies.

2. Methodology

This section first presents the experimental discharge curves. This is followed discussion on the multiphysics model and the optimization of the primary alkaline battery.

2.1 Experimental data

The voltage vs. discharge curves considered in this work are those of an Energizer AA primary alkaline battery as reported in its datasheet (Energizer, 2018). The 250 mA discharge curve was selected due to the moderate discharge current.

2.2 System description

A schematic diagram of the primary alkaline battery is illustrated in Figure 1. At its core is a brass anodic current collector, which draws electrons from the zinc anode during discharge. The zinc anode reacts with OH^- from the KOH electrolyte and oxidizes into $Zn(OH)_4^{2-}$ as shown in Eq(1). The $Zn(OH)_4^{2-}$ ion may precipitate into ZnO if the OH^- concentration is insufficient as given by Eq(2). At the cathode, MnO_2 reacts with water and reduces into MnOOH while generating OH^- as described by Eq(3). Electrons for the cathodic half-reaction are supplied by a steel current collector. The separator is made from polyvinyl alcohol (PVA).

$$\mathrm{Zn(s) + 4OH^-(aq) \rightarrow Zn(OH)_4^{2-}(aq) + 2e^-} \quad (1)$$

$$\mathrm{Zn(OH)_4^{2-}(aq) \rightleftharpoons ZnO(s) + H_2O(l) + 2OH^-(aq)} \quad (2)$$

$$\mathrm{MnO_2(s) + H_2O(l) + e^- \rightarrow MnOOH(s) + OH^-(aq)} \quad (3)$$

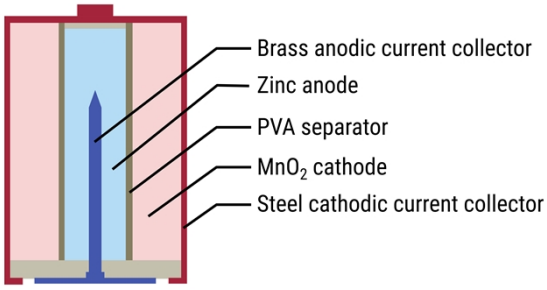

Figure 1: Schematic diagram of a primary alkaline battery.

2.3 Multiphysics model

The multiphysics model of the primary alkaline battery is illustrated in Figure 2. It consists of a 1D axisymmetric model, which describes the mass and charge transport across the battery. This is coupled with particle-scale models for each electrode. The anode has no specific geometry, but the particle-scale model tracks the volume fractions of zinc and ZnO. The cathode is described using a core-shell model with MnO_2 as the core and MnOOH as the shell. The volume fraction of ZnO precipitate is also recorded by the cathode particle-scale model.

The mass and charge transport in the ternary system of K^+, $Zn(OH)_4^{2-}$, and OH^- is modeled by Newman's concentrated solution theory, which considers the interaction between ions unlike the Nernst-Planck equation (Newman and Thomas-Alyea, 2004). The mathematical formulation the mass and charge transport equations

differ for the anode, cathode, and separator, and are detailed by Podlaha and Cheh (1994). The anodic reaction obeys Butler-Volmer kinetics as discussed in the work of Mao and White (1992), while the cathodic reaction kinetics follows the core-shell model described by Podlaha and Cheh, (1994). Precipitation of ZnO occurs when the $Zn(OH)_4^{2-}$ concentration exceeds its equilibrium with OH^-. The formation of ZnO reduces the area available for the anodic and cathodic electrochemical reactions and increases the mass transfer coefficient for ZnO deposition on the electrodes (Podlaha and Cheh, 1994). The model also considers the changing porosities of both electrodes due to the dissolution of zinc, precipitation of ZnO, and conversion of MnO_2 to MnOOH.

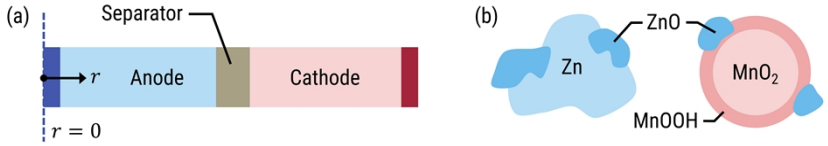

Figure 2: The battery is treated as a 1D axisymmetric system (a). The zinc anode is not modeled as any specific particle geometry, while the MnO_2 cathode is described via a core-shell model MnOOH (b).

2.4 Input model parameters

The input parameters to the multiphysics model are presented in Table 1. The reference current density and diffusion coefficient at the cathode were adjusted to fit experimental data, since the values of these parameters for Energizer's primary alkaline batteries are unknown. Moreover, there is notable uncertainty in these parameters. The reference current density varies with the surface characteristics of the electrode. Meanwhile, the diffusion coefficient in MnO_2 cathodes has a wide range of values in reported literature (Podlaha and Cheh, 1994) and depends on the pore structure of the cathode particle (Farrell and Please, 2005).

Table 1: Input parameters to the multiphysics model.

Parameter	Anode	Separator	Cathode
Thickness [cm]	0.361 [a]	0.025 [a]	0.230 [a]
Diffusivity in the solid phase [$cm^2\ s^{-1}$]	N/A	N/A	8.00×10^{-11} [†]
Diffusivity of $K_2Zn(OH)_4$ [$cm^2\ s^{-1}$]	6.00×10^{-6} [b]	6.00×10^{-6} [b]	6.00×10^{-6} [b]
Diffusivity of KOH [$cm^2\ s^{-1}$]	2.19×10^{-5} [b]	2.19×10^{-5} [b]	2.19×10^{-5} [b]
Transport number of $K_2Zn(OH)_4$	0.04 [c]	0.04 [c]	0.04 [c]
Transport number of KOH	0.74 [c]	0.74 [c]	0.74 [c]
Electrical conductivity of the solid phase [$S\ cm^{-1}$]	1.83×10^{5} (Zn) [c]	0.00 (PVA)	19.8 (MnX) [c]
	0.01 (ZnO) [c]	0.01 (ZnO) [c]	0.01 (ZnO) [c]
Electrical conductivity of the liquid phase [$S\ cm^{-1}$]	Correlation in [c]	Correlation in [c]	Correlation in [c]
Reference current density [$A\ cm^{-2}$]	0.03 [b]	N/A	1.00×10^{-5} [†]
Mass transfer coefficient of ZnO [$cm\ s^{-1}$]	0.005 [c]	0.005 [c]	0.005 [c]
Mass transfer coefficient of $K_2Zn(OH)_4$ [$cm\ s^{-1}$]	0.001 [c]	0.001 [c]	0.001 [c]
Initial concentration of $Zn(OH)_4^{2-}$ [$mol\ cm^{-3}$]	5.34×10^{-4} [c]	5.34×10^{-4} [c]	5.34×10^{-4} [c]
Initial concentration of OH^- [$mol\ cm^{-3}$]	0.007 [c]	0.007 [c]	0.007 [c]
Initial volume fraction of the solid phase	0.26 (Zn) [c]	0.20 (PVA) [c]	0.76 (MnX) [c]
	0.00 (ZnO)	0.00 (ZnO)	0.00 (ZnO)
Initial volume fraction of the liquid phase	0.74 [c]	0.80 [c]	0.24 [c]
Initial volumetric surface area [cm^{-1}]	50 [c]	10 [*]	760 [a]
Equilibrium potential [V]	0	N/A	Correlation in [c]
Equilibrium constant for ZnO dissolution	Correlation in [c]	Correlation in [c]	Correlation in [c]

[*] Assumed [†] Fitted to experiment [a] (Chadderdon and Wendling, 2019) [b] (Mao and White, 1992) [c] (Podlaha and Cheh, 1994)

2.5 Case studies

In the base scenario, the primary alkaline battery was simulated under a 250 mA constant discharge current. The calculated voltage vs. time curve was compared with experimental data to validate the model. In addition, the porosity and concentration profiles in the battery were generated to analyze changes in the battery during discharge. The optimization was performed by simulating the battery under a 250 mA discharge current and 0.8 V cutoff voltage with anode thicknesses from 1 cm to 5 cm. For each anode thickness, the energy capacity was calculated using Eq(4). The anode thickness that results in a battery with the highest energy content was

selected as the optimum. The separator thickness was held constant, while the cathode thicknesses were adjusted so that the total thickness of the battery remains the same as in the base scenario. The porosity and concentration profiles of these batteries were also investigated to determine if the battery's operating mechanism changes with the electrode thicknesses.

$$E = \int_0^{t_{dc}} IV(t)\, dt \tag{4}$$

3. Results and discussion

3.1 Experimental validation

A comparison between the simulated and experimental voltage vs. time data is presented in Figure 3. The discharge curve generated by the model follows the same trend as the experimental data, but the model overpredicts the voltage. Zhang and Cheh (2004) attribute this to the discrepancy between the theoretical (i.e., Nernstian) and actual electric potential of the MnO_2 cathode during discharge. Experiments by Kozawa and Powers (1966) suggest that the deviation is caused by the formation of Mn_2O_3 instead of MnOOH towards the end of discharge. The energy density according to experimental and simulated data are 2.86 Wh and 3.00 Wh, respectively, which corresponds to a 4.93% error in energy density prediction.

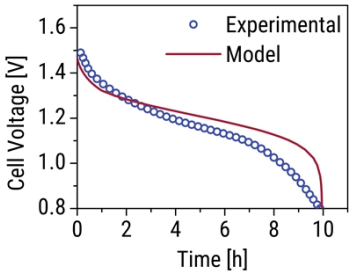

Figure 3: Comparison between experimental and simulated voltage vs. time data.

3.2 Base scenario

The porosity and concentration profiles over time are shown in Figure 4. The porosity profiles show how the solid phase compositions change over time. The ZnO precipitate has a larger molar volume than zinc, so a porosity decrease in the anode and separator indicates a buildup of ZnO. Similarly, MnOOH has a higher molar volume than MnO_2, so a lower porosity implies a higher conversion or utilization of the cathode. ZnO deposition at the cathode is negligible since the high concentration of OH^- dissolves ZnO back into $Zn(OH)_4^{2-}$. The zinc anode dissolves into $Zn(OH)_4^{2-}$ near the anode-separator interface, which in turn precipitates into ZnO throughout the anode and separator. Consequently, the $Zn(OH)_4^{2-}$ concentration profile is maximum at the anode-separator interface, and diminishes towards the left of the anode-separator interface and in the separator. The OH^- concentration rises in the cathode since it is produced by the cathodic reaction, while it decreases in the anode since it is consumed by the anodic reaction. In the anode, the OH^- concentration is highest near the separator since OH^- is produced by the precipitation of $Zn(OH)_4^{2-}$. It is worth noting that the porosity and concentration profiles generated in this work are identical to those obtained by Podlaha and Cheh (1994).

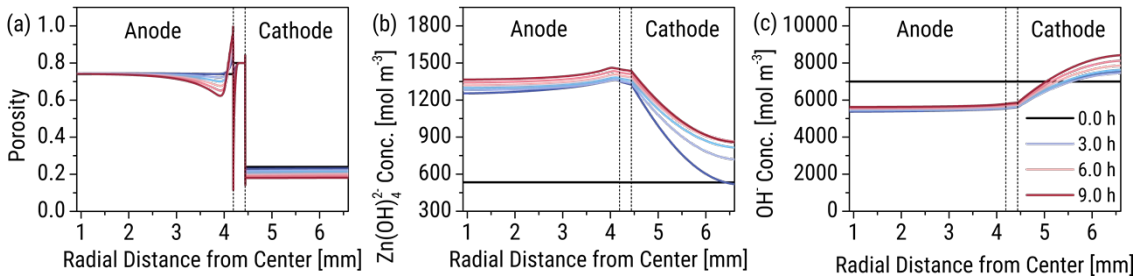

Figure 4: Evolution of the porosity (a), $Zn(OH)_4^{2-}$ concentration (b), and OH^- concentration (c) profiles in the primary alkaline battery over time.

3.3 Optimization scenarios

The energy capacities and discharge curves of primary alkaline batteries with various electrode thicknesses are presented in Figure 5. An anode thickness of 2 cm results in the highest energy density. The 1 cm anode thickness is suboptimal due to discharge suddenly stopping after less than 10 hours of operation. On the other hand, anode thicknesses of 3 cm and greater result in shorter discharge durations because the lower cathode content results in MnO_2 being converted to MnOOH at a faster rate.

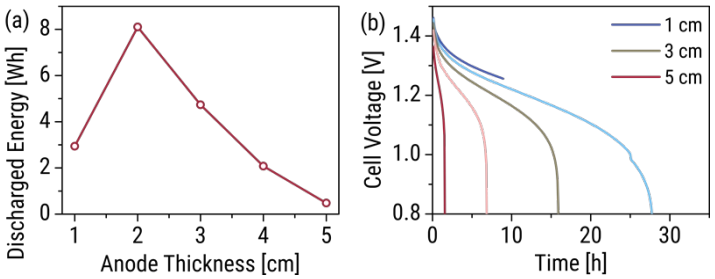

Figure 5: Comparison of the energy capacity (a) and voltage vs. time curves (b) when the anode thicknesses are varied from 1 cm to 5 cm.

The abrupt end of discharge in the battery with a 1 cm anode is explained by the porosity profile shown in Figure 6. The ZnO precipitate builds up at the separator, which stops the ionic current and ends the discharge. The separator is plugged only under the 1 cm anode scenario since the small anode content and large cathode content results in a larger $Zn(OH)_4^{2-}$ concentration increase and a smaller OH^- concentration decrease per coulomb of discharge. The low OH^- concentration cannot stabilize the $Zn(OH)_4^{2-}$, so more precipitation occurs. This would also explain why the minimum porosity increases with the anode thickness.

The porosity profile of the battery with a 2 cm anode thickness shows that the anode dissolves not only at the anode-separator interface, but at the current collector-anode interface as well. This is supported by the uptick of $Zn(OH)_4^{2-}$ and drop-off of OH^- concentrations near the current collector-anode. The additional anode dissolution occurs due the smaller amount of zinc relative to the MnO_2 content. Unfortunately, this increases the likelihood of the zinc anode detaching from the current collector, which would render the anode unusable since current cannot flow towards it. The battery would also cease operating if the anode were to be detached.

An anode thickness of 3 cm would therefore be the best compromise between performance and mechanical stability. Based on the porosity profiles, the zinc anode is consumed near the separator and dissolution near the current collector does not occur. Increasing the anode thickness further diminishes the energy content of the battery since the MnO_2 cathode is exhausted faster as suggested by the porosity profiles.

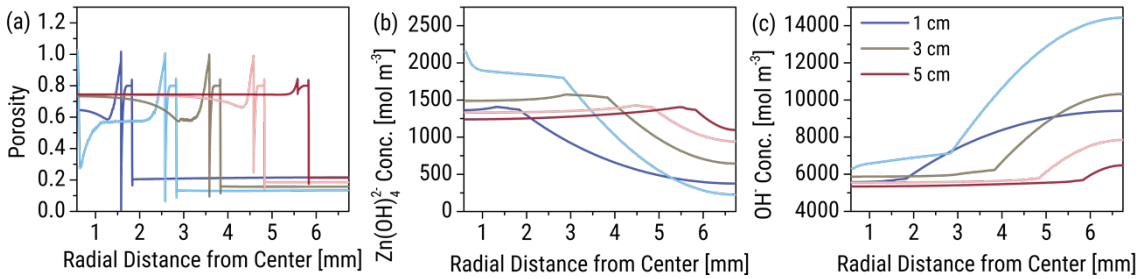

Figure 6: Comparison of the porosity (a), $Zn(OH)_4^{2-}$concentration (b), and OH- concentration (c) profiles at the end of discharge when the anode thicknesses are varied from 1 cm to 5 cm.

4. Conclusions

In this work, the energy capacity of an AA primary alkaline battery was maximized via multiphysics modeling. The multiphysics model of the battery was formulated in COMSOL Mutliphysics®, and this was validated with experimental data published by Energizer Holdings Inc. The reactions and ion transport in the battery were determined by analyzing the porosity and concentration profiles. The optimization was then performed by simulating batteries with various electrode thicknesses while taking note of their energy capacity. The porosity profiles were also observed to reveal any changes in the reaction and ion transport mechanisms.

The multiphysics model was able to replicate the general trend of the experimentally measured voltage vs. time data, although the model tends to overpredict the voltage. The porosity and concentration profiles show that the zinc anode is consumed near the anode-separator interface, while ZnO deposits in the anode and the separator. The optimization study reveals that a 2 cm anode maximizes the energy capacity of the primary alkaline battery, however this also results in the dissolution of the zinc anode at the current collector-anode interface. This would compromise the mechanical stability of the anode, hence a 3 cm anode thickness is recommended, despite its lower energy capacity.

Nomenclature

E – energy capacity, Ah
I – current, A
t – time, h
t_{dc} – discharge time, h
V – voltage, V

Acknowledgments

The authors would like to acknowledge the Department of Science and Technology (DOST) through the Niche Centers in the Regions for R&D (NICER) Program and The Commission on Higher Education – Philippine California Advanced Research Institutes (CHED-PCARI) through the CIPHER Project (IIID 2018-008).

References

Alagheband A., Azimi M., Hashemi H., Kalani M., Nakhaie D., 2017, Optimization of grid configuration by investigating its effect on positive plate of lead-acid batteries via numerical modeling, Journal of Energy Storage, 12, 202–214.

Business Wire, 2020, Alkaline battery report – World market to hrow by USD 493.35 million by 2024, Business Wire <https://www.businesswire.com/news/home/20201104005283/en/> accessed 13.03.2022.

Chadderdon X.H., Wendling M.T., 2019, Mathematical modeling of primary Zn/MnO_2 alkaline batteries, COMSOL <https://www.comsol.com/paper/mathematical-modeling-of-primary-zn-mno2-alkaline-batteries-80991> accessed 13.03.2022.

Edison T.N.J.I., Atchudan R., Karthik N., Xiong D., Lee Y.R., 2019, Direct electro-synthesis of MnO_2 nanoparticles over nickel foam from spent alkaline battery cathode and its supercapacitor performance, Journal of the Taiwan Institute of Chemical Engineers, 97, 414–423.

Energizer, 2018, Product datasheet Energizer E91, Enegizer <http://data.energizer.com/PDFs/E91.pdf> accessed 13.03.2022

Farrell T.W., Please C.P., 2005, Primary alkaline battery cathodes, Journal of The Electrochemical Society, 152, A1930.

Hosseinzadeh E., Marco J., Jennings P., 2017, Electrochemical-thermal modelling and optimisation of lithium-ion battery design parameters using analysis of variance, Energies, 10. 1278.

Kozawa A., Powers R., 1966, The manganese dioxide electrode in alkaline electrolyte: The electron-proton mechanism for the discharge process from MnO_2 to $MnO_{1.5}$, Journal of The Electrochemical Society, 113, 870–878.

Mao Z., White R.E., 1992, Mathematical modeling of a primary zinc/air battery, Journal of The Electrochemical Society, 139, 1105–1113.

Newman J., Thomas-Alyea, K.E., 2004, Electrochemical Systems, John Wiley & Sons, New Jersey, USA.

Podlaha E.J., Cheh H.Y., 1994, Modeling of cylindrical alkaline cells: VII. A wound cell model, Journal of The Electrochemical Society, 141, 1751–1758.

Rarotra S., Sahu S., Kumar P., Kim K.H., Tsang Y.F., Kumar V., Kumar P., Srinivasan M., Veksha A., Lisak G., 2020, Progress and challenges on battery waste management: A critical review, Chemistry Select, 5, 6182–6193.

Samba A., Omar N., Gualous H., Capron O., Van Den Bossche P., Van Mierlo J., 2014, Impact of tab location on large format lithium-ion pouch cell based on fully coupled tree-dimensional electrochemical-thermal modeling, Electrochimica Acta, 147, 319–329.

Seo J.K., Shin J., Chung H., Meng P.Y., Wang X., Meng Y. S., 2018, Intercalation and conversion reactions of nanosized β-MnO_2 cathode in the secondary Zn/MnO_2 alkaline battery, Journal of Physical Chemistry C, 122, 11177–11185.

Sunu W.G., Bennion, D.N., 1980, Transient and failure analyses of the porous zinc electrode: II. Experimental, Journal of The Electrochemical Society, 127, 2017–2025.